

Citation for published version:
Clark, JM, Barpanda, P, Yamada, A & Islam, MS 2014, 'Sodium-ion battery cathodes Na2FeP_O_ and Na2MnP_O_: Diffusion behaviour for high rate performance', *Journal of Materials Chemistry A*, vol. 2, no. 30, pp. 11807-11812. https://doi.org/10.1039/c4ta02383h

10.1039/c4ta02383h

Publication date: 2014

Document Version Peer reviewed version

Link to publication

University of Bath

Alternative formats

If you require this document in an alternative format, please contact: openaccess@bath.ac.uk

Copyright and moral rights for the publications made accessible in the public portal are retained by the authors and/or other copyright owners and it is a condition of accessing publications that users recognise and abide by the legal requirements associated with these rights.

Take down policyIf you believe that this document breaches copyright please contact us providing details, and we will remove access to the work immediately and investigate your claim.

Download date: 09 Mar 2023

Paper

Cite this: DOI: 10.1039/x0xx00000x

Sodium-Ion Battery Cathodes Na₂FeP₂O₇ and Na₂MnP₂O₇: Diffusion Behaviour for High Rate Performance

Received ooth January 2012, Accepted ooth January 2012

DOI: 10.1039/x0xx00000x

www.rsc.org/

John M. Clark, Prabeer Barpanda, Atsuo Yamada, and M. Saiful Islam^{a*}

Na-ion batteries are currently the focus of significant research interest due to the relative abundance of sodium and its consequent cost advantages. Recently, the pyrophosphate family of cathodes has attracted considerable attention, particularly Li₂FeP₂O₇ due to its high operating voltage and enhanced safety properties; in addition the sodium-based pyrophosphates Na₂FeP₂O₇ and Na₂MnP₂O₇ are also generating interest. Herein, we present defect chemistry and ion migration results, determined via atomistic simulation techniques, for Na₂MP₂O₇ (where M = Fe, Mn) as well as findings for Li₂FeP₂O₇ for direct comparison. Within the pyrophosphate framework the most favourable intrinsic defect type is found to be the antisite defect, in which alkali-cations (Na/Li) and M ions exchange positions. Low activation energies are found for long-range diffusion in all crystallographic directions in Na₂MP₂O₇ suggesting three-dimensional (3D) Na-ion diffusion. In contrast Li₂FeP₂O₇ supports 2D Li-ion diffusion. The 2D or 3D nature of the alkali-ion migration pathways within these pyrophosphate materials means that antisite defects are much less likely to impede their transport properties, and hence important for high rate performance.

1. Introduction

Li-ion batteries have dominated the portable energy storage market during the past two decades¹⁻⁷ due to their lightweight, high energy density and high power, which all depend critically on fast Li-ion mobility. Despite the wide-spread use of Li-ion cells, batteries based on alternative carrier ions such as sodium ions could be more suitable for large-scale energy storage systems. Whilst the higher gravimetric capacity afforded by Li-ion cells is critical for portable applications, the relative abundance and low cost associated with Na-ion batteries now make them an attractive alternative for grid storage.^{8,9}

Substantial research effort has been invested during the previous decades to produce electrode materials for sodium batteries that will allow for facile intercalation of Na-ions at suitable potentials. Amongst the cathode materials investigated, a variety of layered oxides (e.g. NaxCO₂, NaCrO₂, NaVO₂, Na_x[Fe_{0.5}Mn_{0.5}]O₂) and polyanionic compounds (e.g. NaFePO₄, Na₃V₂(PO₄)₃, Na₂FePO₄F, NaFeSO₄F) have been reported ¹⁰⁻¹⁷.

Recently lithium pyrophosphate-based materials including Li₂FeP₂O₇ and Li₂Fe $_x$ Mn_{1-x}P₂O₇ (0 $\le x \le$ 1) have been examined, ¹⁸⁻²⁰ which show good electrochemical and thermal properties. It was found that Li₂FeP₂O₇ exhibited a redoxpotential of 3.5 V vs Li/Li⁺ while showing a reversible capacity of ~105 mA h g⁻¹, ¹⁸ whilst for the mixed-metal pyrophosphate it was found that the partial substitution with Mn was observed to

increase the Fe³⁺/Fe²⁺ redox potential.¹⁹ This pyrophosphate structure can offer partial upshift of the Fe³⁺/Fe²⁺ redox potential approaching 4 V (vs Li/Li⁺) independent of cationic size and redox activity of 3d metal substituants.^{21,22} In addition to this high-voltage redox tunability, it is expected that the framework provided by the pyrophosphate anion will give rise to cathode materials with enhanced thermal stabilities.²³

Motivated by the significance of Na-ion batteries for largescale storage systems in addition to the promising properties of Li₂FeP₂O₇, attempts were made to synthesise a sodium version of the Fe-based pyrophosphate (Na₂FeP₂O₇),²⁴⁻²⁶ as well as other Na-analogues with different transition-metal active redox species such as a new Mn-based polymorph, β-Na₂MnP₂O₇.^{27,28} Yamada et al.24 were able to prepare Na2FeP2O7 via a conventional one-step solid-state synthesis, and found it to be electrochemically active, delivering a reversible capacity of 82 mA h g-1 with an operating voltage around 3 V (vs Na/Na+). The combination of low cost materials, moderate theoretical capacity (~100 mA h g⁻¹), high rate kinetics and good thermal stability makes Na₂FeP₂O₇ a highly promising Na-ion battery material. From a crystal structure view-point, the change of alkali ions from Li to Na results in different crystal frameworks: while $\text{Li}_2\text{FeP}_2\text{O}_7$ adopts the monoclinic $(P2_1/c)$ structure¹⁸, Na₂FeP₂O₇ adopts the triclinic (*P*-1) structure²⁵.

Recently β -Na₂MnP₂O₇²⁷ has also been proposed as a new pyrophosphate cathode for sodium-ion batteries, and found to offer similar (if not slightly superior) electrochemical

ARTICLE Journal Name

performance to Na₂FeP₂O₇. Na₂MnP₂O₇ exhibits a discharge capacity close to 80 mA h g⁻¹ (at 25 °C) with a voltage of 3.6 V, the highest Mn³⁺/Mn²⁺ redox potential amongst all Mn-based cathodes. The electrochemical activity of the Mn-containing cathode material is noteworthy, when compared to the Li counterpart (Li₂MnP₂O₇), which is almost inactive at room temperature owing to its sluggish kinetics.²⁸ The β -Na₂MnP₂O₇ polymorph crystallises in the triclinic (P1) space group²⁷, isostructural to the rose-polymorph of Na₂CoP₂O₇.²⁹

The present study uses advanced simulation techniques to investigate important atomic-scale issues related to point defects and alkali (Na/Li) ion migration in Na₂MP₂O₇ (M = Fe, Mn,) and Li₂FeP₂O₇. The present work extends our previous simulation studies of lithium battery electrodes³⁰⁻³⁹ such as LiMPO₄ (M = Mn, Fe, Co, Ni),³¹⁻³⁴ and our investigations of sodium-based cathodes such as NaFeSO₄F³⁶ and Na₂FePO₄F.⁴⁰

2. Simulation Methods

This investigation uses well established simulation techniques based on the Born model of solids. As these techniques are described in detail elsewhere^{41,42}, only a general outline will be given here. All systems were treated as crystalline solids, with interactions between ions consisting of a long-range Coulombic component and a short-range component representing electronelectron repulsion and van der Waals interactions. The shortrange interactions were modelled using the Buckingham potential, 41 and the well-known shell model 43 was employed to account for the polarizability effects. As argued previously, interatomic potential methods are assessed primarily by their ability to reproduce observed crystal properties. Indeed, they are found to work well, even for phosphate and silicate cathodes^{31-36,39} where there is undoubtedly a degree of covalency. The Fe-O, Mn-O, P-O and O-O interatomic potentials were taken directly from the study of the related Li₂FeP₂O₇³⁹ (to which we compare our defect and migration results), whilst the Na-O potential was taken from the recent study of the Na₂FePO₄F⁴⁰ cathode material. The resulting potential parameters are listed in Table S1 (supporting information).

The inclusion of lattice relaxation about defects (such as Na vacancies) and migrating ions was simulated via an implementation of the Mott-Littleton scheme incorporated within GULP (v4.0)⁴⁴. This methodology considers the crystal lattice as two separate regions, with explicit relaxation of the ions in the inner region immediately surrounding the defect (~1000 ions). In contrast, the remainder of the crystal (~3000 ions), where the defect forces are relatively weak, is treated by more approximate quasi-continuum methods.

3. Results and Discussion

3.1 Structural Modelling and Intrinsic Defects

Reproduction of the experimentally observed crystal structures (Figure 1) provided the starting point for the current study. The structure exhibited by Na₂FeP₂O₇ is triclinic (*P*-1),²⁵ comprised of corner-sharing FeO₆ octahedra creating Fe₂O₁₁ dimers, which are interconnected by both corner-sharing and edge-sharing with P₂O₇ pyrophosphate groups. The FeO₆ octahedra and PO₄ tetrahedra are connected in a staggered fashion thus creating large tunnels along the [011] direction within which the Na atoms are present. The Na ions occupy six

distinct crystallographic sites; three of which are fully occupied (Na1, Na2, Na3), whilst the other three adopt sites that are partially occupied (Na4, Na5, Na6). To account for the partial occupancy it was necessary to employ a $3\times1\times1$ supercell approach considering different cation ordering schemes as used in previous simulations. ^{33,36,39} The energetics of the different cation configurations were investigated through a series of geometry optimizations performed under P1 symmetry. We note that the lattice energy differences were found to be very small (< 15 meV), suggesting that any ordering of the Na4, Na5 and Na6 sites may not be significant.

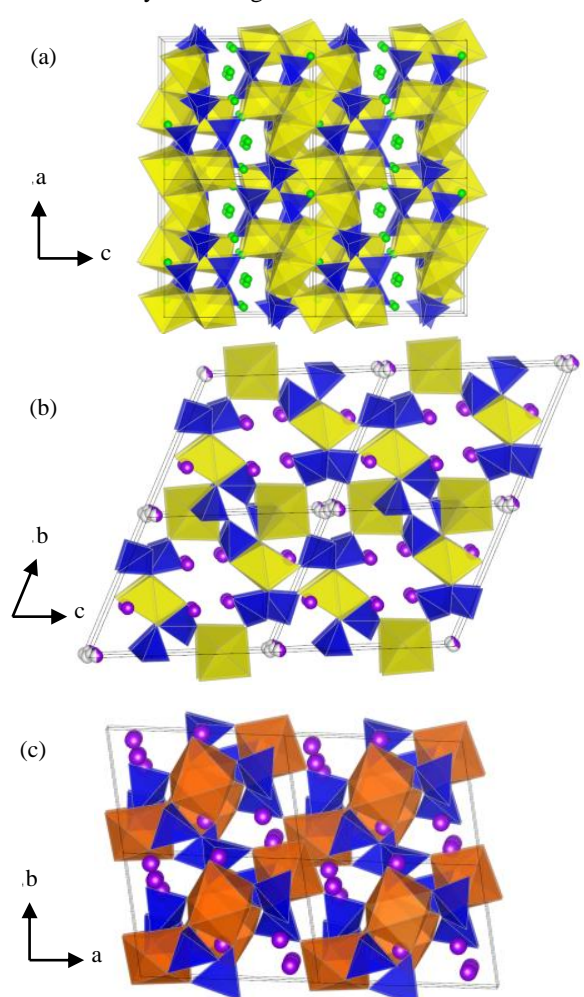


Fig. 1 Crystal structure of Li₂FeP₂O₇ and Na₂MP₂O₇ (M = Fe, Mn). a.) Li₂FeP₂O₇ ($P2_1/c$; c-axis view), b.) Na₂FeP₂O₇ (P-1; a-axis view), c.) Na₂MnP₂O₇ (P1; c-axis view); showing Li ions (green) Na ions (purple), FeO₆ octahedra (yellow), MnO₆ octahedra (orange) and P₂O₇ pyrophosphate units (blue).

The structure exhibited by Na₂MnP₂O₇²⁷ consists of distorted MnO₆ octahedral and tetrahedral building blocks which are connected in a staggered manner thus creating tunnels along the [001] direction. The structures have cornersharing isolated Mn₂O₁₁ dimers, which are in turn connected by the P₂O₇ units by a mixed edge and corner-sharing fashion. The constituent Na atoms are located in eight inequivalent crystallographic sites. It has been postulated that the complex nature of this triclinic (*P*1) structure may allow for multidimensional Na⁺ diffusion.²⁴ Comparisons between the

Journal Name ARTICLE

calculated and experimental crystal structures are given in Table 1.

Table 1 Calculated and Experimental Structural Parameters of Na₂MP₂O₇ (M = Fe, Mn) and $Li_2FeP_2O_7$.

Param	a (Å)	b (Å)	c (Å)	α (°)	β (°)	γ (°)		
$Na_2FeP_2O_7$								
calc.	6.449	9.483	10.993	64.85	86.24	73.13		
expt.25	6.433	9.458	11.143	65.16	85.49	73.49		
Δ (\pm)	0.016	0.025	0.150	0.31	0.75	0.36		
$Na_2MnP_2O_7$								
calc.	9.917	11.169	12.489	148.77	121.26	69.00		
expt.27	9.922	11.084	12.473	148.39	121.95	68.42		
Δ (\pm)	0.005	0.085	0.017	0.38	0.68	0.58		
$\text{Li}_2\text{FeP}_2\text{O}_7^{39}$								
calc.	11.017	9.754	9.805	90.00	101.54	90.00		
expt.	11.200	9.715	9.791	90.00	102.85	90.00		
Δ (±)	0.183	0.039	0.014	0.00	1.31	0.00		

For all pyrophosphate systems, the calculated unit cell parameters deviate from experiment by at most 0.18 Å, and in most cases much less; the same is found for the individual bond lengths. The excellent reproduction of the complex low symmetry monoclinic (Li₂FeP₂O₇) and triclinic (Na₂MP₂O₇) crystal structures gives us confidence that the interatomic potential models can be used reliably in the defect and migration calculations.

Investigation of the defect properties of cathode materials is essential in order to gain a full understanding of their electrochemical behaviour, particularly the possibility of "blocking" antisite defects in structures showing 1D ion conduction. A series of isolated point defect (vacancy and interstitial) energies were calculated for both $Li_2FeP_2O_7$ and $Na_2MP_2O_7$ (M = Fe, Mn). By combining these energies, the relative energies of formation of Frenkel and Schottky type defects were determined. These take the following general forms (using Kröger-Vink notation and where A =Li, Na):

A Frenkel:
$$A_A^X \to V_A' + A_i^{\bullet}$$
 (1)
M Frenkel $M_M^X \to V_M'' + M_i^{\bullet \bullet}$ (2)
O Frenkel $O_0^X \to V_0^{\bullet \bullet} + O_i''$ (3)
Full Schottky $2A_A^X + M_M^X + 2P_P^X + 7O_0^X \to 2V_A' + V_M'' + 2V_P'''' + 7V_0^{\bullet \bullet} + A_2MP_2O_7$ (4)

$$M \text{ Frenkel} \qquad M_M^X \to V_M^{"} + M_i^{\bullet \bullet}$$
 (2)

O Frenkel
$$O_0^X \to V_0^{\bullet \bullet} + O_i^{"}$$
 (3)

Full Schottky
$$2A_A^X + M_M^X + 2P_P^X + 7O_Q^X \rightarrow$$

$$2V_A' + V_M'' + 2V_P''''' + 7V_0^{\bullet \bullet} + A_2MP_2O_7 \tag{4}$$

Calculation of the M/A "antisite" pair defect, involving the exchange of an A⁺ ion (Li⁺ radius 0.76 Å, Na⁺ radius 1.02 Å) with an M^{2+} ion (Fe²⁺ radius 0.78 Å and Mn²⁺ radius 0.83 Å)⁴⁵, was considered according to:

$$M/A$$
 Antisite $M_M^X + A_A^X \rightarrow A_M' + M_A^{\bullet}$ (5)

Analysis of the resulting defect energies listed in Table 2 reveals three main points. First, the magnitude of the calculated energies for M Frenkel, O Frenkel and Schottky defects suggests their formation is unfavourable. Further to which, it is found that O²- vacancies and interstitials are particularly unfavourable, and highly unlikely to occur in any significant concentration in these undoped materials, thus confirming the

structural stability of the pyrophosphate framework in accord with thermal stability experiments²⁵.

Table 2 Energies of Intrinsic Atomic Defect Processes in Na₂MP₂O₇ (M = Fe, Mn) and $Li_2FeP_2O_7$.

		Energy (eV)		
Disorder Type	eq.	$Na_2FeP_2O_7$	$Na_2MnP_2O_7$	$\text{Li}_2\text{FeP}_2\text{O}_7^{39}$
Li or Na Frenkel	(1)	1.14	1.34	1.21
M Frenkel	(2)	3.52	2.93	3.39
O Frenkel	(3)	3.53	3.92	3.99
Full Schottky	(4)	33.03	38.62	32.42
A/M antisite	(5)	0.89	0.80	0.22

Second, the intrinsic defect type found to be most favourable for the Na₂MP₂O₇ material is the Na/M antisite pair as was predicted for the Li/Fe antisite pair in the analogous study of the Li analogue (Li₂FeP₂O₇)³⁹. The formation energy for the Na/M antisite within the Na₂MP₂O₇ materials is of greater magnitude, suggesting lower but still significant concentrations of antisite defects within Na₂MP₂O₇. Since Na⁺ is significantly larger than Li⁺, Fe²⁺ and Mn^{2+ 45}, it is perhaps intuitive that Na/M antisite defect will be less prominent within the pyrophosphate framework than the analogous Li/Fe antisite as revealed by the calculations. Overall our expectation for such defects is that their concentration of antisite disorder would be temperature dependent and therefore sensitive to the experimental conditions imposed during synthesis.

Lastly, the second lowest energies found for the Na₂MP₂O₇ cathode materials were for the Na Frenkel defect formation (Table 2). This result is in accordance with the value calculated for the Li Frenkel defect within Li₂FeP₂O₇³⁹. This suggests that a very minor population of such Li/Na vacancy and interstitial defects could be present at high temperatures. It should be noted that in terms of ion diffusion, the antisite defects will have greater significance within the olivine materials since their presence will block the only available channel for 1D alkali ion migration.31,40

3.2 Na Ion Migration

Examination of the Na⁺ mobility and pathways in Na₂MP₂O₇ is of vital importance when considering their respective charge/discharge rates and any differences with Li+ mobility.

Na-diffusion pathways were considered between all neighbouring Na positions within the Na₂ MP_2O_7 (M = Fe, Mn) materials along each of the three principal axes via conventional vacancy hopping. Energy profiles for Na migration along each of the pathways considered can be mapped out, and the migration energies derived; such an approach has been used in numerous previous studies on oxide ion and cation migration in complex oxides. 31,32,46 The resulting lowest migration energies for Na diffusion along the three principal axes of the Na₂MP₂O₇ materials are reported in Table 3 with the corresponding lowest migration energies for Li diffusion within Li₂FeP₂O₇ reported for comparison³⁹.

From the results presented in Table 3, it would appear that that both Na₂MP₂O₇ structures support quasi-three dimensional (3D) Na⁺ diffusion with activation energies of 0.49 eV and 0.58 eV for Na₂FeP₂O₇, and Na₂MnP₂O₇ respectively. The final calculated paths for long-range Na+ diffusion are shown in Figures 2 and 3. The Li₂FeP₂O₇ compound shows 2D Li⁺ diffusion in the bc-plane with an activation energy of 0.40 eV.³⁹ Therefore in all cases the pyrophosphate framework appears to show high alkali-ion (Na+/Li+) mobility. Although ARTICLE Journal Name

there are no Li $^+$ /Na $^+$ conductivity data for direct comparison, our calculated values for alkali-ion migration are consistent with experimental activation energies for Li/Na ion conductivity in other framework-structured phosphate materials. $^{47\text{-}49}$ We note that in a recent theoretical study of a different Na₂FeP₂O₇ polymorph (triclinic, P1) Na $^+$ diffusion was found to be 2D with migration barriers of ~ 0.54 eV. 26

Table 3 Calculated Migration Energies for Most Favourable Paths of Alkalion Diffusion: Na-ion Migration in Na₂FeP₂O₇ and Na₂MnP₂O₇ and Li-ion Migration in Li₂FeP₂O₇.

Net Diffusion	Migration Energies (eV)					
Direction	$Na_2FeP_2O_7$	$Na_2MnP_2O_7$	$\text{Li}_2\text{FeP}_2\text{O}_7^{39}$			
a-axis	0.33	0.58	0.73			
<i>b</i> -axis	0.42	0.58	0.40			
c-axis	0.49	0.58	0.40			

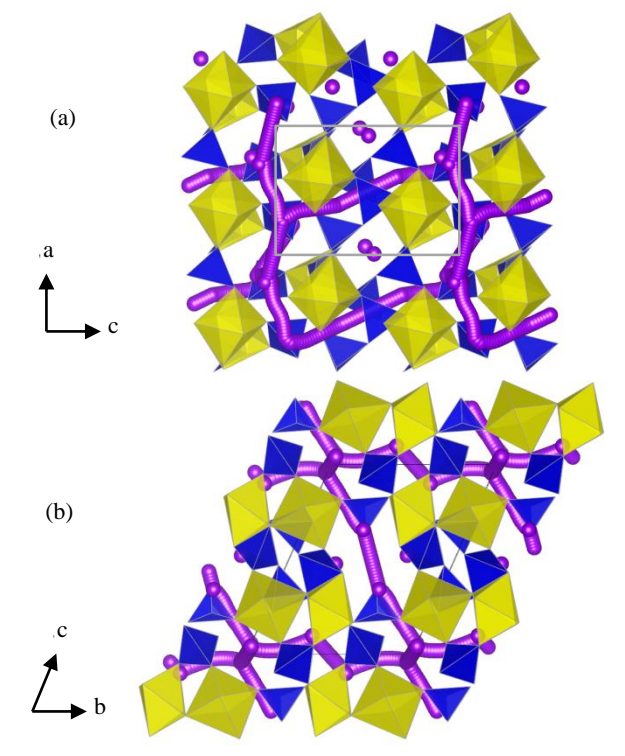


Fig. 2 Calculated paths for long-range Na^+ migration within $Na_2FeP_2O_7$ along the *a*-axis, *b*-axis and *c*-axis directions with activation energies ≤ 0.49 eV; a) view of the *ac*-plane; b) view of the *bc*-plane.

The 2D and 3D transport behaviour in the pyrophosphates contrasts with that in olivine LiFePO₄ and NaFePO₄ which only allow Li⁺/Na⁺ migration along 1D channels parallel to the *b*-axis^{31,40}. In addition, ion blocking by antisite defects is much less likely to make a significant difference to the alkali (Na/Li) ion migration in these pyrophosphate materials. Electrochemical studies indicate that Na₂FeP₂O₇ has excellent rate kinetics, superior to that of Li₂FeP₂O₇³⁹; this may be related to the high dimensionality (3D) and low migration energy for Na-ion diffusion in Na₂FeP₂O₇.

Our simulations also reveal curved paths between adjacent Na/Li sites within each of the pyrophosphate materials studied (Figures 2 and 3). It is worth noting that analogous, curved

migration pathways were first predicted for Li $^+$ diffusion within LiFePO $_4$ based on atomistic calculations, 31 which were subsequently confirmed by neutron diffraction maximum entropy method (MEM) analysis. 50

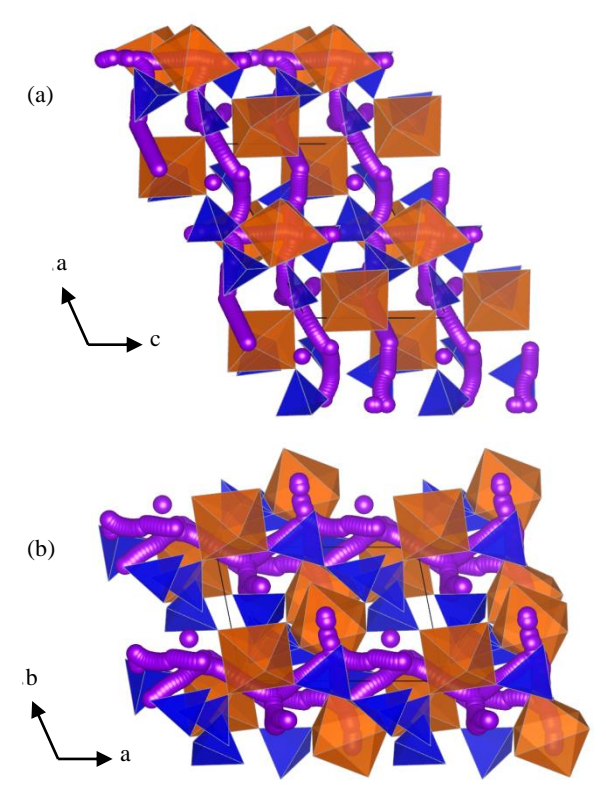


Fig. 3 Calculated paths for long-range Na^+ migration within $Na_2MnP_2O_7$ along the *a*-axis, *b*-axis and *c*-axis directions with activation energies ≤ 0.58 eV; a) view of the *ac*-plane; b) view of the *ab*-plane.

There has been recent debate about the volume difference between the reduced and oxidized phases as a significant factor in determining electrochemical performance of cathode materials. 40,51,52 For two-phase processes, a phase boundary between oxidized and reduced phases is formed during charge/discharge. Electrochemical performance could be affected by the amount of strain generated in this phase boundary, as well as by the activation energy barrier for Li-ion or Na-ion transport.

The difference in the unit cell volume (ΔV) of the oxidized and reduced phases is only ~3.26 % for Na₂FeP₂O₇, but > 15 % for NaFePO₄ and NaFeSO₄F. We note that while the majority of the compounds undergo volume contraction on Li/Na extraction, Li₂FeP₂O₇ shows a small volume expansion, although de(lithiation) has been found to be via a solid-solution mechanism in this pyrophosphate⁵². Although the interplay of all factors is still under investigation, materials with a large volume difference between the end member phases could lead to poor rate capability as discussed by Tripathi et al⁴⁰. In contrast, promising electrochemical properties can be anticipated for Na-based cathode materials with low volume change on cycling (e.g. < 7 %) and low ion migration activation barriers (e.g. < 0.5 eV) as in the case of Na₂FeP₂O₇ and Na₂FePO₄F.

4. Conclusions

Journal Name ARTICLE

We have investigated Fe- and Mn- based pyrophosphate materials which offer promising high rate cathodes that are potentially low cost and thermally stable for sodium-ion batteries. This survey of Na₂MP₂O₇ (M = Fe, Mn) with comparison to Li₂FeP₂O₇ used atomistic simulation techniques to provide insights into their defect and ion migration properties.

First, the simulations show good reproduction of the observed complex structures of $Na_2FeP_2O_7$ and $Na_2MnP_2O_7$. The defect calculations indicate the stability of the pyrophosphate framework towards oxygen evolution, which is important for operational safety. The most favourable intrinsic defect type is the Na/M and Li/Fe antisite, with the relative energies suggesting greater Li/Fe disorder in the $Li_2FeP_2O_7$ material as observed.

Secondly, both Na₂FeP₂O₇ and Na₂MnP₂O₇ are predicted to exhibit curved diffusion pathways parallel to the *a*-, *b*- and *c*-axes with low migration energies (~0.50 eV). Hence, the pyrophosphate framework appears to support 3D Na⁺ diffusion in Na₂MP₂O₇, (and 2D Li⁺ diffusion in Li₂FeP₂O₇), which is consistent with the high rate kinetics observed for Na₂FeP₂O₇.

Acknowledgements

This work was funded by the EPSRC Supergen programme and made use of the high-performance computing service HECTOR, via the HPC Materials Chemistry Consortium. PB thanks the Japan Society for the Promotion of Sciences for a JSPS Fellowship. VESTA⁵³ was used for analysis of results.

Notes and references

- ^a Department of Chemistry, University of Bath, Bath, BA2 7AY, United Kingdom.
- Department of Chemical System Engineering, School of Engineering,
 The University of Tokyo, 7-3-1 Hongo, Bunkyo-Ku, Tokyo 113-8656,
 Japan.
- ^c Materials Research Center, Indian Institute of Science, Bangalore 560012, India.
- ^d Unit of Element Strategy Initiative for Catalysts & Batteries, ESICB, Kyoto University, Kyoto 615-8510, Japan.
- \dagger Electronic Supplementary Information (ESI) available: [details of any supplementary information available should be included here]. See DOI: 10.1039/b000000x/
- 1. M. Armand, J. M. Tarascon, Nature 2008, 451, 652.
- 2. J. B. Goodenough, Y. Kim, Chem. Mater. 2010, 22, 587.
- 3. B. L. Ellis, K. T. Lee, L. F. Nazar, Chem. Mater. 2010, 22, 691.
- 4. M. R. Palacin, Chem. Soc. Rev. 2009, 38, 2565.
- 5. C. Masquelier, L. Croguennec Chem. Rev. 2013, 113, 6552.
- V. Etacheri, R. Marom, R. Elazari, G. Salitra, D. Aurbach, Energy Environ. Sci. 2011, 4, 3243.
- 7. Z. L. Gong, Y. Yang, Energy Environ. Sci. 2011, 4, 3223.
- 8. B. L. Ellis, L. F. Nazar, Curr. Opin. Solid State Mater. Sci. 2012, 16, 168
- 9. V. Palomares, P. Serras, I. Villaluenga, K. B. Hueso, J. Carretero-Gonzalez, T. Rojo, *Energy Environ. Sci.* **2012**, *5*, 5884.
- C. Delmas, J. J. Braconnier, C. Fouassier, P. Hagenmuller, Solid State Ionics 1981, 4, 165.
- S. Komaba, C. Takei, T. Nakayama, A. Ogata, N. Yabuuchi, *Electrochem. Commun.* 2010, 12, 355.
- N. Yabuuchi, M. Kajiyama, J. Iwatate, H. Nishikawa, S. Hitomi, R. Okuyama, R. Usui, Y. Yamada, S. Komaba, *Nat. Mater.* 2012, 11, 512.
- P. Moreau, D. Guyomard, J. Gaubicher, F. Boucher, *Chem. Mater.* 2010, 22, 4126.

 Z. L. Jian, L. Zhao, H. L. Pan, Y. S. Hu, H. Li, W. Chen, L. Q. Chen, *Electrochem. Commun.* 2012, 14, 86.

- J. Barker, M. Y. Saidi, J. L. Swoyer, Electrochem. Solid State Lett. 2003, 6, A1.
- B. L. Ellis, W. R. M. Makahnouk, Y. Makimura, K. Toghill, L. F. Nazar, *Nat. Mater.* **2007**, *6*, 749.
- P. Barpanda, J. N. Chotard, N. Recham, C. Delacourt, M. Ati, L. Dupont, M. Armand, J. M. Tarascon, *Inorg. Chem.* 2010, 49, 7401.
- S. Nishimura, M. Nakamura, R. Natsui, A. Yamada, J. Am. Chem. Soc. 2010, 132, 13596.
- N. Furuta, S. Nishimura, P. Barpanda, A. Yamada, *Chem. Mater.* 2012, 24, 1055.
- M. Tamaru, P. Barpanda, Y. Yamada, S. Nishimura, A. Yamada, J. Mater. Chem. 2012, 22, 24526.
- T. Ye, P. Barpanda, S. Nishimura, N. Furuta, S. C. Chung, A. Yamada, *Chem. Mater.* **2013**, *25*, 3623.
- P. Barpanda, M. Ati, B. C. Melot, G. Rousse, J. N. Chotard, M. L. Doublet, M. T. Sougrati, S. A. Corr, J. C. Jumas, J. M. Tarascon, *Nat. Mater.* 2011, 10, 772.
- M. Tamaru, S. C. Chung, D. Shimizu, S. Nishimura, A. Yamada, *Chem. Mater.* 2013, 25, 2538.
- P. Barpanda, T. Ye, S. Nishimura, S. C. Chung, Y. Yamada, M. Okubo, H. S. Zhou, A. Yamada, *Electrochem. Commun.* 2012, 24, 116
- P. Barpanda, G. Liu, C. D. Ling, M. Tamaru, M. Avdeev, S. C. Chung, Y. Yamada, A. Yamada, Chem. Mater. 2013, 25, 3480.
- 26. H. Kim, R. A. Shakoor, C. Park, S. Y. Lim, J. S. Kim, Y. N. Jo, W. Cho, K. Miyasaka, R. Kahraman, Y. Jung, W. J. Choi, *Adv. Funct. Mater.* 2013, 23, 1147.
- P. Barpanda, T. Ye, M. Avdeev, S. C. Chung, A. Yamada, *J. Mater. Chem. A* 2013, *1*, 4194.
- C. S. Park, H. Kim, R. A. Shakoor, E. Yang, S. Y. Lim, R. Kahraman,
 Y. Jung, W. J. Choi, J. Am. Chem. Soc. 2013, 135, 2787.
- 29. F. Erragh, A. Boukhari, E. Elouadi, E. M. Holt, *J. Crystallogr. Spectrosc. Res.* **1991**, *21*, 321.
- 30. C. Eames, A. R. Armstrong, P. G. Bruce, M. S. Islam, *Chem. Mater.* **2012**, *24*, 2155.
- M. S. Islam, D. J. Driscoll, C. A. J. Fisher, P. R. Slater, *Chem. Mater.* 2005, 17, 5085.
- C. A. J. Fisher, V. M. H. Prieto, M. S. Islam, M. S. Chem. Mater. 2008, 20, 5907.
- 33. G. R. Gardiner, M. S. Islam, Chem. Mater. 2010, 22, 1242.
- 34. C. A. J. Fisher, M. S. Islam, J. Mater. Chem. 2008, 18, 1209.
- 35. A. R. Armstrong, N. Kuganathan, M. S. Islam, P. G. Bruce, *J. Am. Chem. Soc.* **2011**, *133*, 13031.
- R. Tripathi, G. R. Gardiner, M. S. Islam, L. F. Nazar, *Chem. Mater.* 2011, 23, 2278.
- 37. N. Kuganathan, M. S. Islam, Chem. Mater. 2009, 21, 5196.
- 38. A. R. Armstrong, C. Lyness, P. M. Panchmatia, M. S. Islam, P. G. Bruce, *Nat. Mater.* **2011**, *10*, 223.
- J. M. Clark, S. Nishimura, A. Yamada, M. S. Islam, *Angew. Chem. Int. Ed.* 2012, 51, 13149.
- R. Tripathi, S. M. Wood, M. S. Islam, L. F. Nazar, *Energy Environ. Sci.* 2013, 6, 2257.
- A. Walsh, A. A. Sokol, C. R. A. Catlow, Computational Approaches to Energy Materials. In Wiley-Blackwell, 2013.
- 42. M. S. Islam, C. A. J. Fisher, Chem. Soc. Rev. 2014, 43, 185.
- 43. B. G. Dick, A. W. Overhauser, Phys. Rev. 1958, 112, 90.
- 44. J. D. Gale, A. L. Rohl, Mol. Simul. 2003, 29, 291.
- 45. R. D. Shannon, Acta Crystallogr. 1976, A32, 751.
- 46. M. S. Islam, P. R. Slater, MRS Bull. 2009, 34, 935.
- C. Delacourt, L. Laffont, R. Bouchet, C. Wurm, J. B. Leriche, M. Morcrette, J. M. Tarascon, C. Masquelier, *J. Electrochem. Soc.* 2005, 152, A913.
- J. Y. Li, W. L. Yao, S. Martin, D. Vaknin, Solid State Ionics 2008, 179, 2016.
- 49. L. Sebastian, J. Gopalakrishnan, J. Mater. Chem. 2003, 13, 433.
- S. Nishimura, G. Kobayashi, K. Ohoyama, R. Kanno, M. Yashima, A. Yamada, *Nat. Mater.* 2008, 7, 707.
- 51. Y. Zhu, Y. Xu, Y. Liu, C. Luo, C. Wang, Nanoscale 2013, 5, 780.
- D. Shimizu, S. Nishimura, P. Barpanda, A. Yamada, *Chem. Mater.* 2012, 24, 2598.
- 53. K. Momma, F. Izumi, J. Appl. Crystallogr. 2008, 41, 653.